Lin *et al. Robotics and Biomimetics* (2014) 1:24
DOI 10.1186/s40638-014-0024-1

Robotics and Biomimetics
a SpringerOpen Journal

RESEARCH Open Access

Path planning of mechanical polishing process for freeform surface with a small polishing tool

Weiyang Lin[1,2,3], Peng Xu[1,4], Bing Li[1*] and Xiaojun Yang[1]

Abstract

Products with freeform surface are widely applied in industries, and the surface quality plays an important role in order to fulfill the targeted functions. As polishing path of small polishing tool affects the polishing removal function considerably, it is highly necessary to study the polishing path of freeform surface for obtaining good polishing efficiency and well-proportioned surface quality. By combining the Preston polishing removal function, the material removal model of small polishing tool under the control of constant polishing force and pressure is established. Based on this model, the material removal functions of scan line, Archimedean spiral, and Hilbert fractal polishing path are derived. The simulation results show that the Hilbert fractal polishing path has the best comprehensive performance. By using the projection relation of differential geometry, the optimal path generation algorithm of the Bézier surface based on Hilbert fractal polishing path is established. The polishing experiments are conducted on a self-developed polishing machine which is based on a parallel manipulator. The experimental results demonstrate that the surface roughness is improved from level 9 to level 11.

Keywords: Mechanical polishing; Small polishing tool; Freeform surface; Polishing path; Removal function

Background

Product structure can be optimized by using freeform surfaces, which opens the door for solutions with improved performance, reduced complexity, lower mass, and smaller size. However, due to the geometric particularity, freeform surfaces face more challenges and difficulties in precision manufacturing. Polishing is usually one of the final processing steps of precision manufacturing, and the results directly affect the appearance and longevity of parts [1]. It is fundamentally different from other precision manufacturing technologies. Removal of polishing does not only depend on the position of the tool orthogonal to the workpiece, as for grinding and cutting processes but also proportional to the product of local pressure and relative-speed between tool and workpiece and the dwell time. In recent years, there were efforts to develop versatile polishing processes in order to achieve high accuracy. The current polishing methods mainly include electrochemical polishing [2], magnetorheological fluid polishing [3,4], plasma polishing [5,6], ultrasonic polishing [7,8] and computer-controlled mechanical polishing [9,10]. Nowadays, a lot of freeform components are still produced by final manual polishing. It not only heavily relies on the know-how and experience of technicians but also needs much attention for processing and testing. To achieve a given level of precision with high efficiency and reliability, process automation is clearly the way forward. As the computer-controlled mechanical polishing has high efficiency and can be controlled easily [11], it is the focus of this study. The mechanical polishing is a statistical 'rubbing' process that the microscopic loose-abrasive particles in the polishing liquid which is driven by high-speed rotational polishing tool could produce friction with the part surface. Protruding portions of the surface are removed to meet the roughness requirement. However, due to the various factors, the polishing process heavily relies on trial and experience, which leads to a slow development in the mechanical polishing process.

Compared with the large polishing tool, the small polishing tool used in this study has many advantages [12]. The small tool can follow the freeform surface with relatively large curvature, while large tool cannot polish the freeform surface with curvature smaller than its radius. The small tool can redress the error of local surface, while

*Correspondence: libing.sgs@hit.edu.cn
[1] Shenzhen Graduate School, Harbin Institute of Technology, Shenzhen University Town, Xili, 518055 Shenzhen, China
Full list of author information is available at the end of the article

a large tool may polish the nearby surface when it polishes a local surface. The small can also operate at greater pressure and velocity than a large tool; therefore, it can remove the material in a rapid manner. In the case of manufacturing one single piece, small polishing tool has a higher polishing efficiency.

As the polishing surface is highly nondeterministic, one of the reasons is that the polishing path of the tool affects the removal considerably. A basic requirement for polishing paths is that the surface can be completely and uniformly covered during a polishing cycle. Therefore, the study of removal function of different polishing path has a very important significance. A lots of polishing paths in mechanical polishing process can be found in literatures [13-18]. The ultimate goal of the research about different polishing removal function is to select an optimal polishing path so as to avoid any under-polishing and over-polishing phenomenon and ensure the uniformity of the polishing process. Meanwhile, it can also present a clear understanding of the various factors that influence the polishing quality. The core issue of this research is to study the polishing removal function and the polishing performance in a given surface shape and a specified path, so that it can facilitate the subsequent polishing path control.

The rest of the paper is organized as follows. In the 'Theoretical background' section, some basic polishing assumptions and fundamental theories are introduced. In the 'Methods' section, the scan line path, Archimedean spiral path, and Hilbert fractal path are described and analyzed in details, while the modeling method of polishing path from plane surface to freeform surface is also given. The simulation and experiment are conducted, and the results are depicted in the 'Results and discussion' section. Conclusions are drawn in the last section.

Theoretical background

Removal rate of polishing

Removal rate of polishing, which depicts the properties of part surface's removal amount at a local polishing position during every unit of time, is an important part of study about polishing process [19,20]. Many factors affect the polishing removal rate, such as polishing tool and polishing environment [21-23]. For the polishing tool, the main factors are material property, shape, and surface roughness. While for the polishing part, the results are relevant to material property and friction coefficient between the part and the polishing tool. Additionally, for the polishing environment, the main factors include the particle size and viscosity of polishing paste and polishing liquid, the temperature and pressure during polishing and the chemical correction of part in the polishing liquid.

Preston presented theoretical basis for the prediction of material removal for mechanical polishing [18]. Although there are many other polishing formulations in polishing literatures, most of them are based on the Preston equation. Tseng and Wang [24] proposed a modification equation based on the Preston equation in chemical-mechanical polishing; Nanz [25] considered the bending of pad and flow of slurry into the Preston equation to obtain a new polishing formula. The formula of Preston polishing removal function is displayed as below:

$$f(\vec{q},t)=\frac{\mathrm{d}z}{\mathrm{d}t}=k\cdot p(\vec{q},t)\cdot v(\vec{q},t) \tag{1}$$

where $f(\vec{q},t)$ is the material removal in unit time; $\vec{q}$ is the position vector of polishing point; t is the time; k is the Preston coefficient which is related to the material, polishing liquid, and environment; $p(\vec{q},t)$ is the pressure at the polishing point; and $v(\vec{q},t)$ is the instantaneous polishing velocity at the polishing point.

Actually, the problem of polishing removal rate is a very complex nonlinear problem. Preston polishing removal function is a linearization assumption, but it is approximately valid in many practical polishing experiments.

Removal amount of polishing path

In terms of mechanical polishing, the polishing velocity and polishing pressure can be controlled by computer numerical control (CNC) machine precisely. Therefore, during the polishing process, the Preston coefficient k is regarded as constant. Moreover, the polishing tool is usually made of relatively soft materials. At the micro level, the soft tool is adaptive to the shape of surface. It can keep the polishing tool and word-piece contact with each other throughout the polishing process. Thus, the polishing pressure applied by small polishing tool on freeform surface is assumed to be uniform; that is to say, the pressure of contact surface is equal everywhere at the same time.

At time τ and point $\vec{q}$ in the part coordinate system, the polishing velocity and pressure are set as $v(\vec{q},\tau)$ and $n(\tau)$, respectively. When the radius of polishing tool is R, the polishing removal amount is defined as follow:

$$z(x,y,t)=\int_0^t k\cdot\frac{n(\tau)}{2\pi\cdot R^2}\cdot v(\vec{q},\tau)\mathrm{d}\tau \tag{2}$$

The polishing pressure during the polishing process can be divided into the constant polishing pressure n_s and the time-varying polishing pressure $n_v(\tau)$, namely $n(\tau)=n_s+n_v(\tau)$. However, in order to simplify the subsequent discussion, we assume that the polishing force remains constant during the polishing process. Then, the polishing removal function can be rewritten as:

$$z(x,y,t)=\frac{k\cdot n_s}{2\pi\cdot R^2}\cdot\int_0^t v(\vec{q},\tau)\mathrm{d}\tau \tag{3}$$

Equation 3 is a general polishing removal function. Given different polishing paths, the polishing velocity

in Equation 3 will change correspondingly, and this will result in different integration results.

Removal function at a fixed point

Figure 1 is the diagram of polishing model at a fixed point. When the polishing tool is stationary and rotates with angular velocity ω_t, the polishing removal function of the point with radius r to the center of polishing tool is described as:

$$z(r,t) = \frac{k \cdot n_s}{2\pi \cdot R^2} \cdot r \cdot \omega_t \cdot t \tag{4}$$

The Equation 4 is a conical surface as shown in Figure 2. The velocity of polishing tool center equals zero which results in zero removal amount at this point.

In practice, the polishing velocity is the sum of feed velocity and rotation velocity; that is to say, $v = v_t + r \cdot \omega_t$. However, the angular velocity ω_t of the polishing tool is very large which can reach about thousands of revolutions per minute. As a result, v_t is very small and $r \cdot \omega_t \gg v_t$, so it can be considered that $v \approx r \cdot \omega_t$.

Methods

Tool paths are one of the key factors for the automatic mechanical surface polishing. Three polishing paths are covered in this study: scan line path, Archimedean spiral path, and Hilbert fractal path. How they affect the polishing results are investigated here.

Scan line polishing path

The scan line path, a conventional machining path, is frequently used in CNC machining. In the scan line polishing process, the polishing tool offsets an interval at the boundary and continues the machining until the processing is done.

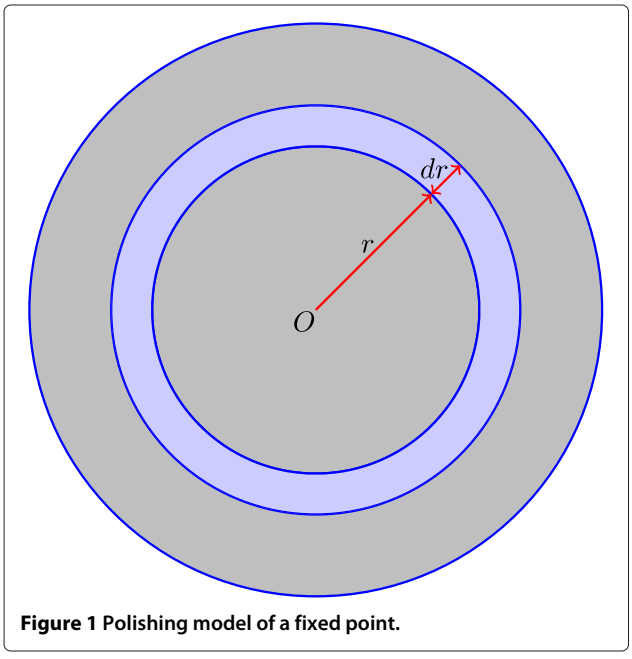

Figure 1 Polishing model of a fixed point.

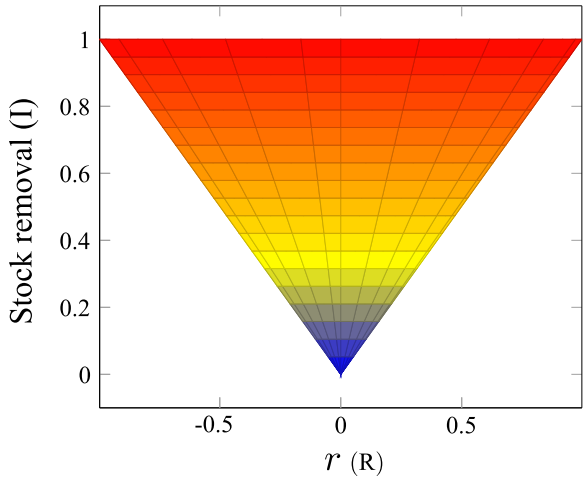

Figure 2 Removal function of a fixed point.

Removal function of single line polishing path

In the modeling of single line polishing path along the X-axis, the removal function Equation 3 at point (x_p, y_p) on plane can be rewritten as:

$$\begin{aligned} z(x_p, y_p) &= \frac{k \cdot n_s}{2\pi \cdot R^2} \cdot \int_0^{\infty} v(\vec{q}(x(\tau), y_p), \tau) d\tau \\ &= \frac{k \cdot n_s}{2\pi \cdot R^2} \cdot \int_{-\frac{\sqrt{r^2 - y_p^2}}{v_t}}^{\frac{\sqrt{r^2 - y_p^2}}{v_t}} \omega_t \cdot \sqrt{(v_t \tau)^2 + y_p^2}\, d\tau \\ &= \frac{k \cdot n_s}{2\pi \cdot R^2} \cdot \frac{\omega_t}{v_t} \cdot \left[R\sqrt{R^2 - y_p^2} \right. \\ &\quad \left. + y_p^2 \left(\ln\left(R + \sqrt{R^2 - y_p^2} \right) - \ln(|y_p|) \right) \right] \end{aligned} \tag{5}$$

where $y_p \in [-R, R]$.

The coefficient term of Equation 5 is proportional to the removal function, and it does not impact the shape of the removal function curve. Thus, let I represent the coefficient term:

$$I = \frac{k \cdot n_s}{2\pi \cdot R^2} \cdot \frac{\omega_t}{v_t} \tag{6}$$

Figure 3 is the removal function of single line polishing path in the XZ plane. The maximum removal value is not at the polishing tool center, although the center point has a longest valid polishing length.

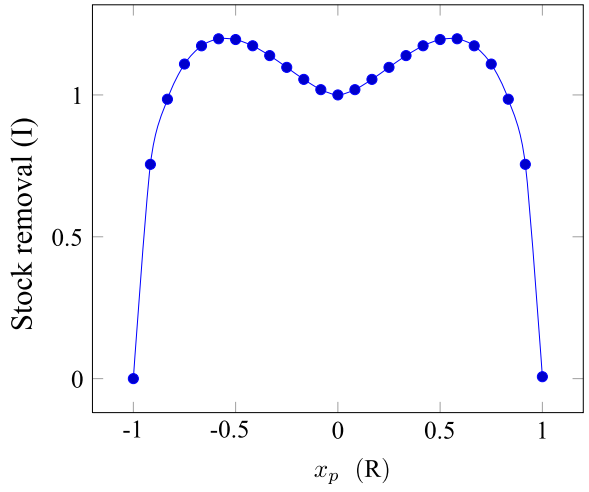

Figure 3 Removal function of single line polishing path.

Removal function of scan line polishing path

Figure 4 is the polishing model of scan line path. L denotes the interval of two adjacent lines. Equation 5 can be rewritten as the following piecewise function:

$$Z_s(x,y) = \begin{cases} I \cdot \left(R\sqrt{R^2-y^2} + y^2 \left(\ln(R+\sqrt{R^2-y^2}) - \ln(|y|) \right) \right), & y \in [-R,R] \\ 0, & y \notin [-R,R] \end{cases} \tag{7}$$

Let $Z_{y_0}(x,y) = Z_s(x,y-y_0)$ denote removal function of the polishing line $y = y_0$. Calculating the sum of all the polishing lines with interval L, the removal function of scan line is:

$$Z(x,y) = \sum_{i=-n}^{n} Z_{(i\cdot L)}(x,y) \tag{8}$$

Archimedean spiral polishing path

Archimedean spiral is an arithmetic spiral, which is one of the most useful machining paths. Due to the rotational motion of workpiece, with no need of reversing, the polishing machine can achieve smooth and steady motion.

Modeling of Archimedean spiral polishing path

Figure 5 is the model of Archimedean spiral polishing path. Let L be the constant separation distance and v_t be the feed velocity of the polishing tool. The Archimedean spiral formula in the polar coordinate system is $\rho = (L \cdot \theta)/2\pi$. The feed velocity of polishing tool is $v_t = \sqrt{\dot{\rho}^2 + \rho^2\omega^2}$. Therefore, the angular velocity of the Archimedean spiral $\omega = \dot{\theta}$ can be obtained:

$$\dot{\theta} = \frac{2\pi v_t}{L} \cdot \frac{1}{\sqrt{1+\theta^2}} \tag{9}$$

With the initial condition $\theta(0) = 0$, the integral for Equation 9 is:

$$\theta\sqrt{1+\theta^2} + \operatorname{arcsinh}(\theta) = \frac{4\pi}{L} \cdot v_t t \tag{10}$$

where $\operatorname{arcsinh}(\theta) = \ln\left(\theta + \sqrt{1+\theta^2}\right)$ is the inverse hyperbolic function. There is no analytical expression for θ in Equation 10. The value of θ should be calculated by numerical method and then the value of ρ can be obtained.

Figure 6 is the model of Archimedean spiral polishing path. R is the radius of the polishing tool and r is the distance between point (ρ_0, θ_0). (ρ, θ) denotes the polishing tool center. According to the cosine law $r(\rho, \theta, \rho_0, \theta_0) =$

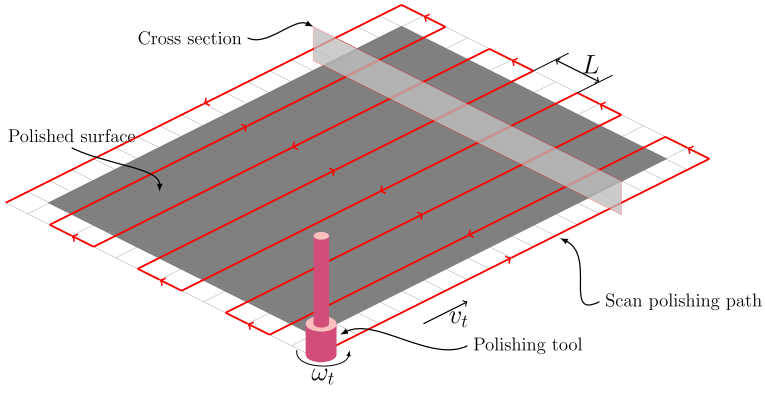

Figure 4 Scan line polishing path.

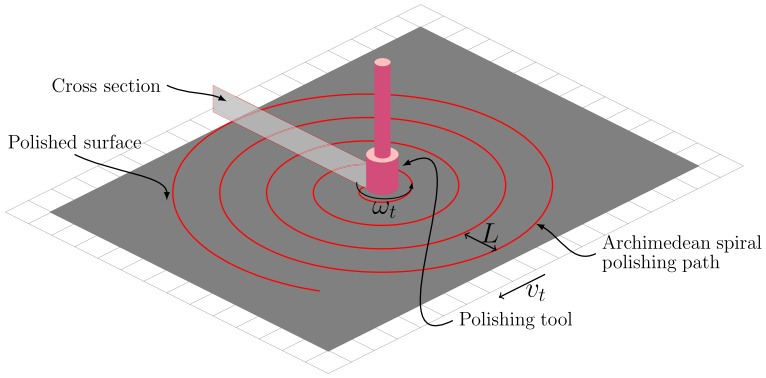

Figure 5 Archimedean spiral polishing path.

$\sqrt{\rho^2+\rho_0^2-2\rho\rho_0\cos(\theta-\theta_0)}$, the polishing velocity v_R of the polishing point (ρ,θ) can be expressed as:

$$v_R(\rho,\theta,\rho_0,\theta_0)=\sigma_R\left[r(\rho,\theta,\rho_0,\theta_0)\right]\cdot\omega_t \tag{11}$$

where the piecewise function σ_R is defined as follows:

$$\sigma_R=\begin{cases} r, & |r|\le R \\ 0, & |r|>R \end{cases} \tag{12}$$

For a given velocity v_t and a separation distance L, the variables ρ and θ are the function of t. With Equations 3 and 11, the integral of Archimedean spiral path can be obtained as:

$$Z(\rho_0,\theta_0)=I\cdot v_t\cdot\int_0^{\infty}\sigma_R \times\left(\sqrt{\rho(\tau)^2+\rho_0^2-2\rho(\tau)\rho_0\cos(\theta(t)-\theta_0)}\right)d\tau \tag{13}$$

The polishing process of Archimedean spiral is the uniform motion polishing process, the natural coordinate is $s=v_t\cdot t$. Thus, Equations 10 and 13 can be rewritten as:

$$\theta\sqrt{1+\theta^2}+\operatorname{arcsinh}(\theta)=\frac{4\pi}{L}\cdot s \tag{14}$$

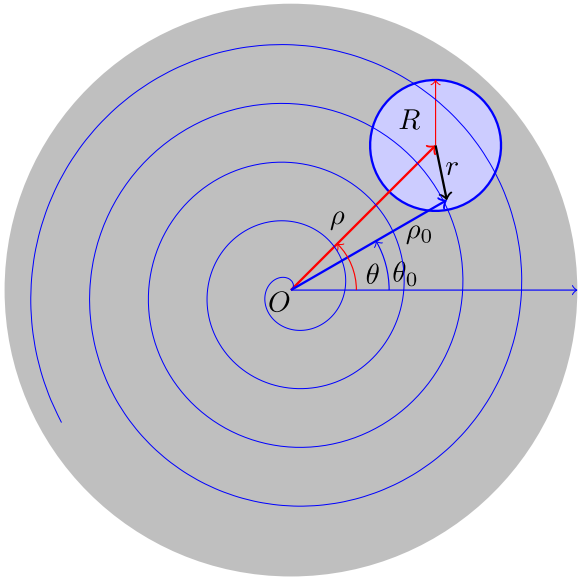

Figure 6 Polishing model of Archimedean spiral path.

$$Z(\rho_0,\theta_0)=I\cdot\int_0^{\infty}\sigma_R \times\left(\sqrt{\rho(s)^2+\rho_0^2-2\rho(s)\rho_0\cos(\theta(s)-\theta_0)}\right)ds \tag{15}$$

In the natural coordinate system, Archimedean spiral path is expressed by natural coordinate s rather than time t.

Removal function of Archimedean spiral polishing path

The expression of natural coordinate s can be obtained from Equation 14:

$$s=\frac{L}{4\pi}\left[\theta\sqrt{1+\theta^2}+\operatorname{arcsinh}(\theta)\right] \tag{16}$$

Set the radius of the polishing tool R as a reference unit 1. The polar coordinate of polishing tool center is (ρ,θ). Let $s_e=s(\rho_0+R)$; $s_o=s(\rho_0-R)$ in condition $\rho_0>R$, and $s_o=0$ in condition $\rho_0\le R$. s_o and s_e are the new

lower and upper limits of Equation 15. Thus, the removal function can be obtained with new limits:

$$Z(\rho_0,\theta_0) = I \cdot \int_{s_o}^{s_e} \sigma_R \times\left(\sqrt{\rho(s)^2+\rho_0^2-2\rho(s)\rho_0\cos(\theta(s)-\theta_0)}\right) ds \tag{17}$$

Using numerical method and discrete method, the removal function of Equation 17 can be rewritten approximately as:

$$Z(\rho_0,\theta_0) = I \cdot \sum_{s_o}^{s_e} \sigma_R \times\left(\sqrt{\rho(s)^2+\rho_0^2-2\rho(s)\rho_0\cos[\,\theta(s)-\theta_0]}\right)\Delta s \tag{18}$$

The value of Equation 18 at polishing point (ρ_0,θ_0) can be calculated by Newton's method.

Hilbert fractal polishing path

The scan line and Archimedean spiral polishing path discussed above are very directional. Therefore, the removal functions of them have strong anisotropy property. The anisotropy property destroys the polishing isotropy of the polished surface. In order to obtain high polishing quality, the removal function of designed polishing path with isotropy property is expected to apply into freeform surface polishing task.

Fractal curve

The fractal curve refers to the curve with fractal dimension. The local simple structure of fractal curve is suitable for CNC programming and controlling, while the global randomness property shows a global isotropy characteristic to remove the streaks of polished freeform surface and improves the polishing quality.

Fractal curves include snowflake fractal curve, triangle fractal curve, Hilbert fractal curve, and so on, but not every fractal curve is qualified for surface polishing. The qualified fractal curve needs to satisfy the following conditions: surface ergodic property, easy motion control for CNC, and strong isotropy property.

The surface ergodic property requires the fractal path with dimension greater than one, and the fractal curve can cover the polished surface when the order of the fractal curve is large enough. In mathematics, it means that the closure of the fractal curve is homeomorphism to two-dimensional plane.

The surface ergodic property requires that fractal curve can cover the whole higher-order polished surface. The snowflake fractal curve does not fulfill the surface ergodic property. For example, the cubic Koch snowflake cannot cover the two-dimensional surface. On the other hand, the easy motion control property requires the simple curve. The isometric segment is a good choice for this requirement because of easy planning, programming, and CNC machining. The snowflake fractal curve does not have well isotropic property globally, and it has a strong global orderliness with the high orders. Hence, it is not suitable for polishing purpose. Fulfilling the three requirements for freeform surface polishing, the Hilbert fractal curve is selected for freeform surface polishing here.

As shown in Figure 7, the Hilbert fractal path is organized with segments and traverses the whole two-dimensional plane. The segments of the Hilbert curve are parallel to X axis or Y axis. They can be easily controlled by CNC machine. Also, Hilbert fractal path has a good isotropy and no orderliness in global.

Modeling of Hilbert fractal polishing path

Figure 8 is the polishing model of the Hilbert curve. Similar to the scan line and Archimedean spiral polishing path, let ω_t and ν_t denote the rotational velocity and the feed velocity in polishing process, respectively.

The basic unit of the Hilbert curve is segment. Therefore, Equation 3 with segment path can be applied for Hilbert polishing path. The segments of Hilbert curve are all parallel to X axis or Y axis.

For a given segment along X axis direction, the motion of polishing tool center is uniform linear motion in segment $C_x\left[(x_s,y)-(x_e,y)\right]$. The removal function is nonnegative. Hence, changing the integral variable from $\mathrm{d}\tau$ to $\mathrm{d}x$ needs to use absolute function to guarantee the nonnegative value of Equation 3. The removal function on point $(x_\mathrm{p},y_\mathrm{p})$ generated by the polishing segment C_x can be obtained:

$$Z_{C_x}(x_\mathrm{p},y_\mathrm{p},y) = I \cdot \left|\int_{x_s}^{x_e} \sigma_R\left(\sqrt{(x-x_\mathrm{p})^2+(y-y_\mathrm{p})^2}\right) dx\right| \tag{19}$$

Similarly, $C_y\,[(x,y_s)-(x,y_e)]$ denotes the uniform linear segment of polishing tool center along Y axis direction, the removal function on point $(x_\mathrm{p},y_\mathrm{p})$ generated by the polishing segment C_y can be obtained as:

$$Z_{C_y}(x_\mathrm{p},y_\mathrm{p},x) = I \cdot \left|\int_{y_s}^{y_e} \sigma_R\left(\sqrt{(x-x_\mathrm{p})^2+(y-y_\mathrm{p})^2}\right) dy\right| \tag{20}$$

The σ_R in Equations 19 and 20 has a mutation at the point where $|r| = R$. Therefore, the mutation is not convenient for solving the integration of Equations 19 and 20. x_- and x_+ are the x-coordinate of intersection points

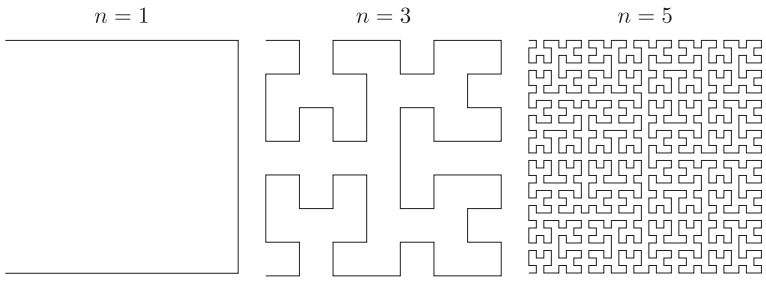

Figure 7 Hilbert fractal path.

between the line and the circle. Let $X_{\min} = \min(x_s, x_e)$ and $X_{\max} = \max(x_s, x_e)$; let $x_- = x_\mathrm{p} - \sqrt{R^2 - (y - y_\mathrm{p})^2}$ and $x_+ = x_\mathrm{p} + \sqrt{R^2 - (y - y_\mathrm{p})^2}$ under condition $|y - y_\mathrm{p}| \le R$. The valid lower and upper limits $x'_s \le x'_e$ of integral function along X axis direction the polishing segment can be defined as:

$$x'_s = \begin{cases} x_- , & X_{\min} \le x_- \le X_{\max}, \text{ and } |y - y_\mathrm{p}| \le R \\ X_{\min} , & x_- \le X_{\min} \le x_+, \text{ and } |y - y_\mathrm{p}| \le R \\ \text{not defined} , & \text{other} \end{cases} \tag{21}$$

$$x'_e = \begin{cases} x_+ , & X_{\min} \le x_+ \le X_{\max}, \text{ and } |y - y_\mathrm{p}| \le R \\ X_{\max} , & x_- \le X_{\max} \le x_+, \text{ and } |y - y_\mathrm{p}| \le R \\ \text{not defined} , & \text{other} \end{cases} \tag{22}$$

Similarly, let $Y_{\min} = \min(y_s, y_e)$ and $Y_{\max} = \max(y_s, y_e)$; let $y_- = y_\mathrm{p} - \sqrt{R^2 - (x - x_\mathrm{p})^2}$ and $y_+ = y_\mathrm{p} + \sqrt{R^2 - (x - x_\mathrm{p})^2}$ under condition $|x - x_\mathrm{p}| \le R$. The valid lower and upper limits $y'_s \le y'_e$ of integral function along Y axis direction polishing segment can be defined as:

$$y'_s = \begin{cases} y_- , & Y_{\min} \le y_- \le Y_{\max}, \text{ and } |x - x_\mathrm{p}| \le R \\ Y_{\min} , & y_- \le Y_{\min} \le y_+, \text{ and } |x - x_\mathrm{p}| \le R \\ \text{not defined} , & \text{other} \end{cases} \tag{23}$$

$$y'_e = \begin{cases} y_+ , & Y_{\min} \le y_+ \le Y_{\max}, \text{ and } |x - x_\mathrm{p}| \le R \\ Y_{\max} , & y_- \le Y_{\max} \le y_+, \text{ and } |x - x_\mathrm{p}| \le R \\ \text{not defined}, & \text{other} \end{cases} \tag{24}$$

The integrands of Equations 19 and 20 are given, respectively:

$$f_{x_\mathrm{p}, y_\mathrm{p}}(x, y) = \frac{\delta x \sqrt{\delta x^2 + \delta y^2} + \delta y^2 \ln\left(\delta x + \sqrt{\delta x^2 + \delta y^2}\right)}{2} \tag{25}$$

$$g_{x_\mathrm{p}, y_\mathrm{p}}(x, y) = \frac{\delta y \sqrt{\delta x^2 + \delta y^2} + \delta x^2 \ln\left(\delta y + \sqrt{\delta x^2 + \delta y^2}\right)}{2} \tag{26}$$

where $\delta x = x - x_\mathrm{p}$, $\delta y = y - y_\mathrm{p}$.

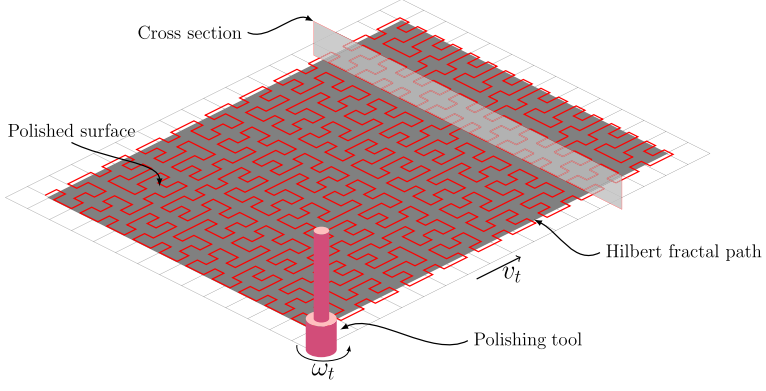

Figure 8 Hilbert fractal polishing path.

When x in $f_{x_p,y_p}(x,y)$ is not defined, $f_{x_p,y_p}(x,y) = 0$; when y in $g_{x_p,y_p}(x,y)$ is not defined, $g_{x_p,y_p}(x,y) = 0$. With new defined lower and upper limits, the absolute function can be removed from the integration. The single uniform linear polishing segment can be rewritten as:

$$Z_X\left(x_p,y_p,x_s,x_e,y\right) = I\cdot\left|f_{x_p,y_p}\left(x'_e,y\right) - f_{x_p,y_p}\left(x'_s,y\right)\right| \tag{27}$$

$$Z_Y\left(x_p,y_p,x,y_s,y_e\right) = I\cdot\left|g_{x_p,y_p}\left(x,y'_s\right) - g_{x_p,y_p}\left(x,y'_s\right)\right| \tag{28}$$

where x'_s, x'_e, y'_s, and y'_e are defined in Equations 21, 22, 23, and 24.

Applying uniform linear motion segment, the removal functions of Equations 27 and 28 with the Hilbert fractal curve are the segments set **H**, the removal function of Hilbert fractal curve at point (x_p, y_p) is the sum of all the segments removal functions:

$$\begin{aligned} Z\left(x_p,y_p\right) = &\sum_{C_{X_i}\in\mathbf{H}} Z_{X_i}\left(x_p,y_p,x_{si},x_{ei},y_i\right) \\ &+ \sum_{C_{Y_j}\in\mathbf{H}} Z_{Y_j}\left(x_p,y_p,x_j,y_{sj},y_{ej}\right) \end{aligned} \tag{29}$$

Freeform surface polishing modeling

The previous polishing paths are all discussed in the planer plane. Referring to differential geometry method, the planer plane can be mapped on a freeform surface. The following discusses the general mapping method.

Natural coordinate expression of freeform surface path

The freeform curve expressed by natural coordinate s can be directly used in path planning. Freeform surface refers to a smooth two-dimensional surface with finite or infinite degrees of freedom. Because the order of freeform

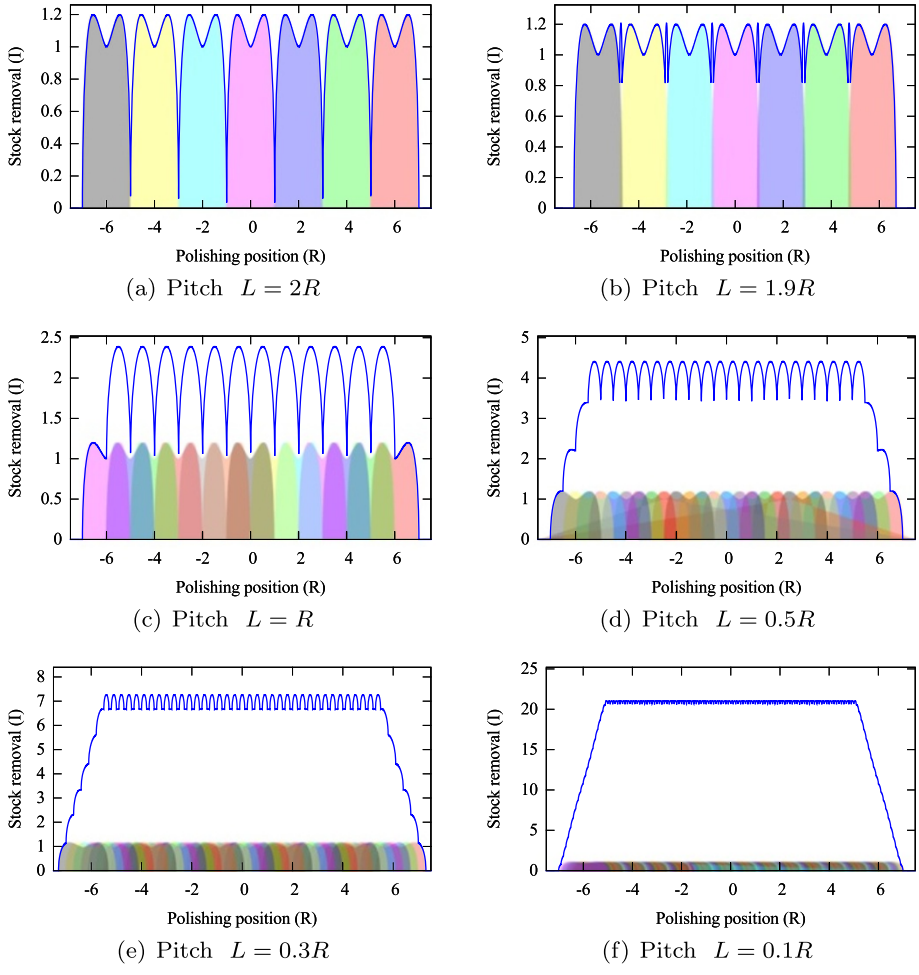

Figure 9 Removal function of scan line path with different spaces. (a) Pitch $L = 2R$, **(b)** $L = 1.9R$, **(c)** $L = R$, **(d)** $L = 0.5R$, **(e)** $L = 0.3R$, **(f)** $L = 0.1R$.

surface is unknown, it can hardly use an unified expression to describe the surface exactly. The freeform surface is expressed by linear combining of several basic functions to approach the freeform surface itself. The polynomial is one of the most useful basic functions due to its simpleness and easy calculation. According to the approximation theory, piecewise polynomial surfaces can approximate a smooth freeform surface in arbitrary precision.

Let C_{uv} be polishing path in parameter u-v plane and t be the parameter of path C_{uv}. Mapping the plane to the freeform surface obtains the project path C_f. The space path C_f can be expressed as follows:

$$x = x(u(t), v(t)),\ y = y(u(t), v(t)),\ z = z(u(t), v(t)) \tag{30}$$

In application, $x(t)$ and $y(t)$ are selected as the parameter variables of $u(t)$ and $v(t)$. The path C_f on freeform surface is described as $z = z\,(x(t),\ y(t))$.

The natural coordinate parameter s which is the length of curve is used to replace the parameter variable t to describe the space path C_f. Referring to formula $\mathrm{d}s = \sqrt{\mathrm{d}x^2 + \mathrm{d}y^2 + \mathrm{d}z^2}$, natural coordinate parameter s can be written as:

$$s = \int_0^t \sqrt{\left(1 + z_x^2\right) x_t^2 + 2 z_x z_y x_t y_t + \left(1 + z_y^2\right) y_t^2} \cdot \mathrm{d}\tau \tag{31}$$

where $z_x = \mathrm{d}z/\mathrm{d}x$.

With Equation 31, the interpolation algorithm of the polishing path on freeform surface can be easily designed.

Modeling of polishing path on the Bézier freeform surface

The traditional surface fitting methods include the Hermite method, Bézier method, B-spline method, and NURBS method. The Bézier surface can approximate any freeform surface and has fewer parameters which make it easier to use in practice. Thus, the Bézier method is studied in this paper for freeform surface polishing.

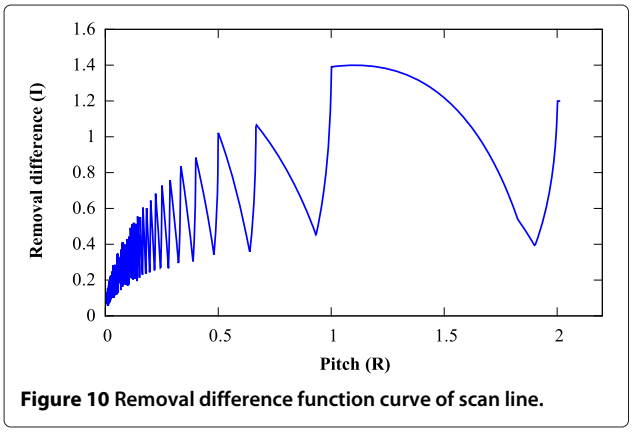

Figure 10 Removal difference function curve of scan line.

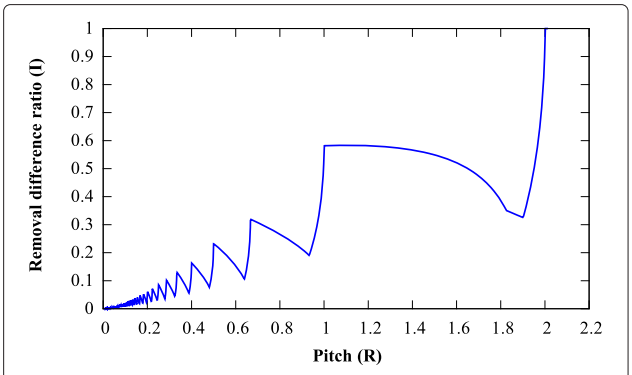

Figure 11 Removal difference ratio function curve of scan line.

Bézier method is polynomial-based approximation algorithm. The degree n of the polynomial is related to the number of the knots. Polynomial can approximate a smooth function in arbitrary precision. Hence, the polynomial-based Bézier surface can approximate the smooth freeform surface as well in arbitrary precision.

Given m rows and n columns Bézier control points $P_{ij} = \left[P_{ij}^x, P_{ij}^y, P_{ij}^z\right]$. Let $\mathbf{B}_{k-1}(\alpha) = \left[B_{k-1}^0(\alpha), B_{k-1}^1(\alpha), \cdots, B_{k-1}^{k-1}(\alpha)\right]^{\mathrm{T}}$, $\mathbf{P}_{mn}^x = \left\{P_{ij}^x\right\}$, $\mathbf{P}_{mn}^y = \left\{P_{ij}^y\right\}$, and $\mathbf{P}_{mn}^z = \left\{P_{ij}^z\right\}$. Thus, the Bézier surface can be expressed as:

$$\begin{cases} x(u,v) = \mathbf{B}_{m-1}^{\mathrm{T}}(u) \cdot \mathbf{P}_{mn}^x \cdot \mathbf{B}_{n-1}(v) \\ y(u,v) = \mathbf{B}_{m-1}^{\mathrm{T}}(u) \cdot \mathbf{P}_{mn}^y \cdot \mathbf{B}_{n-1}(v) \\ z(u,v) = \mathbf{B}_{m-1}^{\mathrm{T}}(u) \cdot \mathbf{P}_{mn}^z \cdot \mathbf{B}_{n-1}(v) \end{cases} \tag{32}$$

where $u \in [0, 1]$, $v \in [0, 1]$.

The Bernstein basic function $B_n^i(\alpha)$ is defined as:

$$B_n^i(\alpha) = \sum_{i=0}^{n} \frac{n!}{i!\,(n-i)!} (1-\alpha)^{n-i} \alpha^i \tag{33}$$

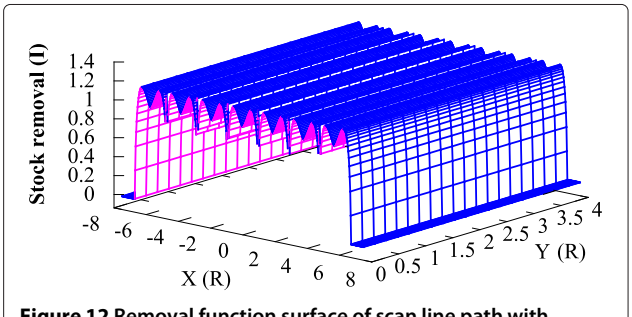

Figure 12 Removal function surface of scan line path with interval 1.9*R*.

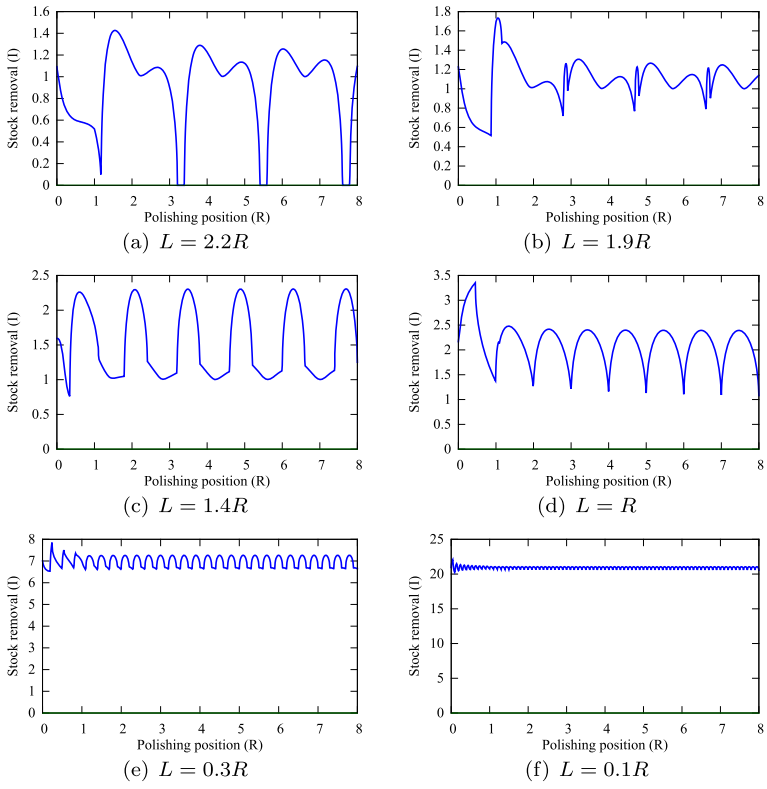

Figure 13 Removal function of Archimedean spiral path with different spaces at $\theta = 0$. **(a)** $L = 2.2R$, **(b)** $L = 1.9R$, **(c)** $L = 1.4R$, **(d)** $L = R$, **(e)** $L = 0.3R$, **(f)** $L = 0.1R$.

Set the Bézier surface with the range of $[X_s, X_e] \times [Y_s, Y_e]$. The affine transformation from u-v to x-y is defined as:

$$u = (x - X_s)/(X_e - X_s) \quad , \quad v = (y - Y_s)/(Y_e - Y_s) \quad (34)$$

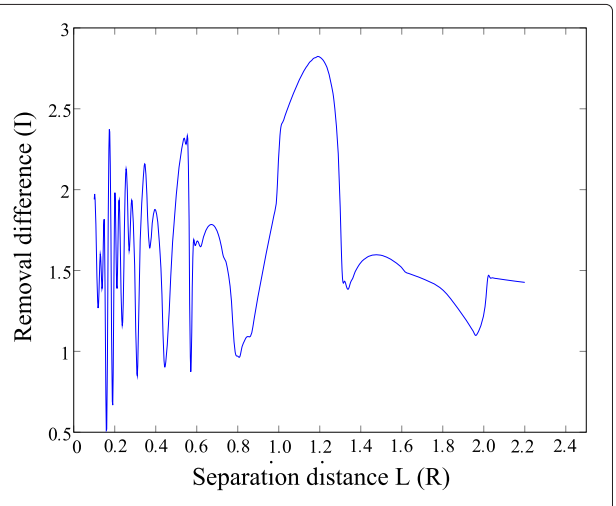

Figure 14 Removal difference function of the Archimedean spiral.

The surface is evenly divided into $m \times n$ matrix points. Therefore, $P_{ij}^x = X_s + \frac{i-1}{m-1} \cdot (X_e - X_s)$ and $P_{ij}^y = Y_s + \frac{j-1}{n-1} \cdot (Y_e - Y_s)$. Bernstein polynomial is endowed with a binomial expansion $\sum_{i=0}^{n} B_n^i(\alpha) = 1$. The identical relation for the $x(u, v)$ and $y(u, v)$ in Equation 32 is:

$$\begin{cases} x\left(\dfrac{x - X_s}{X_e - X_s}, t\right) & = x \\ y\left(t, \dfrac{y - Y_s}{Y_e - Y_s}\right) & = y \end{cases} \quad (35)$$

The Bézier surface can be simplified as follows:

$$z(x, y) = \mathbf{B}_{m-1}^{\mathrm{T}}\left(\frac{x - X_s}{X_e - X_s}\right) \cdot \mathbf{P}_{mn}^z \cdot \mathbf{B}_{n-1}\left(\frac{y - Y_s}{Y_e - Y_s}\right) \quad (36)$$

Thus, z_x and z_y in Equation 31 are expressed as:

$$z_x = \mathbf{B}_{m-1}'^{\mathrm{T}}\left(\frac{x - X_s}{X_e - X_s}\right) \cdot \mathbf{P}_{mn}^z \cdot \mathbf{B}_{n-1}\left(\frac{y - Y_s}{Y_e - Y_s}\right) \quad (37)$$

$$z_y = \mathbf{B}_{m-1}^{\mathrm{T}}\left(\frac{x - X_s}{X_e - X_s}\right) \cdot \mathbf{P}_{mn}^z \cdot \mathbf{B}_{n-1}'\left(\frac{y - Y_s}{Y_e - Y_s}\right) \quad (38)$$

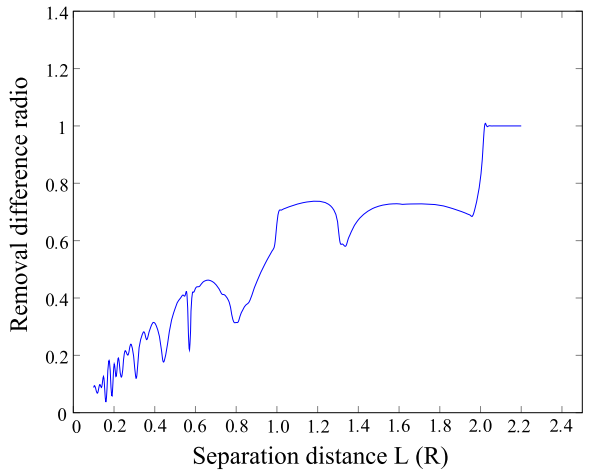

Figure 15 Removal difference ratio function curve of Archimedean spiral.

The first order derivative of Bernstein function is $B_n^{i\prime}(t) = n\left[B_{n-1}^{i-1}(t) - B_{n-1}^{i}(t)\right]$. Hence, $\mathbf{B}'^{\mathrm{T}}_{m-1}\left(\frac{x-X_s}{X_e-X_s}\right)$ and $\mathbf{B}'_{n-1}\left(\frac{y-Y_s}{Y_e-Y_s}\right)$ can be calculated by a series of simple algebraic operation. With the natural coordinate parameter s, the interpolation algorithm of freeform surface curve can be directly obtained.

Results and discussion

Different parameters for the same type of polishing path may cause different quality. The following will discuss removal function of the different polishing paths and optimize the parameters of the polishing path.

Simulation

Scan line polishing path

Figure 9 shows the removal function curves of the scan line polishing with different spaces L. Ignoring the boundary effect, the points on the surface have no more than two times of repeatedly polishing along the feed direction when $R < L < 2R$. However, when $L < R$, there are several times of repeatedly polishing of the surface. If the equivalent coefficient and the ratio between the rotational speed and the feed speed of polishing tool is fixed, the polishing

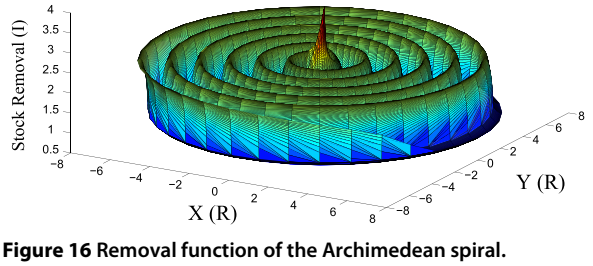

Figure 16 Removal function of the Archimedean spiral.

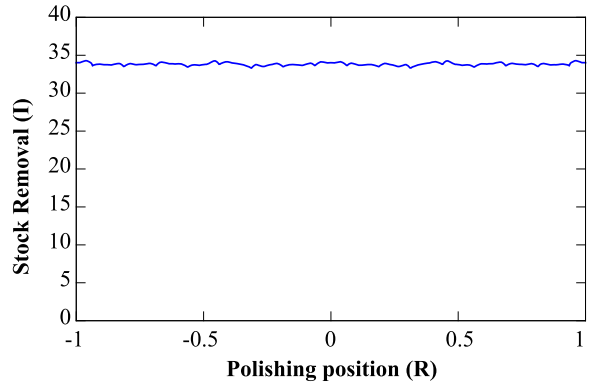

Figure 17 Removal function graph of five-order Hilbert curve along the X axis.

removal amount and the uniformity will increase with the decrease of the polishing space $L < R$. As the main role of polishing is to remove the microscopic irregularities of the surface, the smaller removal amounts the better the surface uniformity based on the condition that the accuracy of polishing is ensured.

Set the maximum removal amount and the minimum removal amount at a specific polishing point during a polishing cycle as $Z_{\max}$ and $Z_{\min}$, respectively. The difference of the removal amount $\Delta Z = Z_{\max} - Z_{\min}$ which is varied with polishing space is studied. By numerical calculation, the curve of the ΔZ changed with polishing space can be obtained as shown in Figure 10. It displays that the removal amount increases with the decrease of the polishing space according to a zigzag trend. By only considering the difference of removal amount and eliminating the effect of the removal amount, it can be seen that the smaller polishing space has a better polishing results. Of

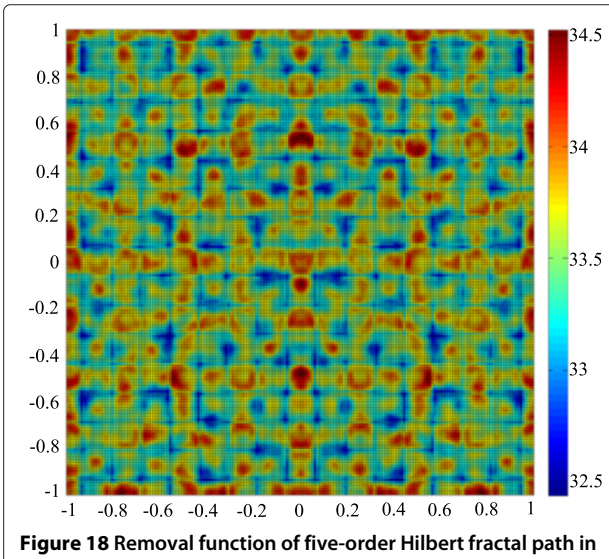

Figure 18 Removal function of five-order Hilbert fractal path in the XY plane.

Table 1 Feature comparison of the polishing path

Polishing type	Uniformity	Isotropy	Motion control	Comprehensive review
Scan line	Bad	Bad	Easy	Easy control, low polishing quality
Archimedean spiral	Bad	General	Hard	Hard control, general polishing quality
Hilbert curve	Good	Good	General	Easy control, high polishing quality

course, this value needs to be selected from the trough point on the zigzag curve.

The uniformity of the polishing cannot be fully seen if only the difference of the polishing removal amount ΔZ is discussed, because different polishing space has different difference maximum polishing amount $Z_{\max}$. Thus, the difference ratio coefficient $R_{\Delta Z} = \Delta Z/Z_{\max}$ is introduced to eliminate the effect of $Z_{\max}$ on ΔZ. Figure 11 shows that the ratio coefficient $R_{\Delta Z}$ varies with the polishing space. Although the trend of the results is similar to the curve line of the polishing removal amount during a cycle, Figure 11 can better reflect the polishing amount uniformity of the polishing path.

In order to ensure the polishing efficiency and avoid excessive repeatedly polishing of the surface, the polishing space should be set within the interval of $[R, 2R]$. From Figures 10 and 11, it can be found that the optimal value appear in the vicinity of $1.9R$. The planar graph and the three-dimensional graph of the removal function at this value is shown in Figure 9b and Figure 12, respectively.

Archimedean spiral polishing path

Figure 13 shows that the curves of the polishing removal function vary with ρ_0 when $\theta_0 = 0$. When $L > 2R$, the spiral polishing path do not interfere with each other. Thus, the curve of removal function is an independent waveform. Similar to the scan line polishing path, the polishing amount increased with the decrease of the polishing space. What different to the scan line polishing path is that the Archimedean spiral polishing path displays quasi-periodicity characteristic. The periodicity becomes increasingly stronger with the distance from the center of Archimedean spiral path and the removal amount near the center of the Archimedean spiral path varies considerably.

In order to depict the uniformity of the Archimedean spiral polishing, $Z_{\max}$ is set as the maximum removal amount and $Z_{\min}$ is set as the minimum removal amount. The difference of the removal amount is represented as $\Delta Z = Z_{\max} - Z_{\min}$. By numerical calculation, ΔZ changing with the space can be derived as shown in Figure 14. Different from the scan line polishing path, the smaller polishing space does not display a better polishing results.

The difference ratio coefficient $R_{\Delta Z} = \Delta Z/Z_{\max}$ is introduced, and the curve line that it varies with the polishing space is shown in Figure 15. It can be seen from the figure that with the decrease of the polishing space, the uniformity of the surface becomes better and better.

In practical, the polishing space of the Archimedean spiral cannot tend to zero. In order to improve the polishing efficiency, the polishing space usually set within the interval of $[R, 2R]$. Figure 16 demonstrates the three-dimensional graph of removal function at the optimal polishing space $L = 1.3R$ which can be obtained from

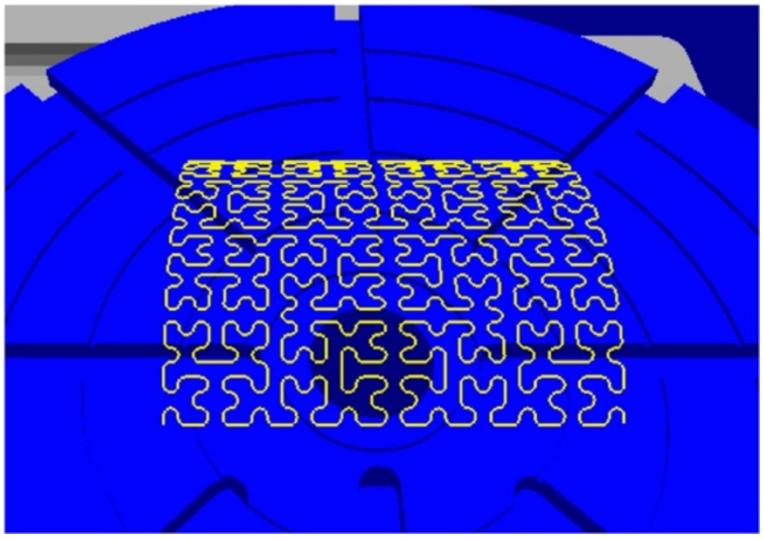

Figure 19 Hilbert fractal polishing path.

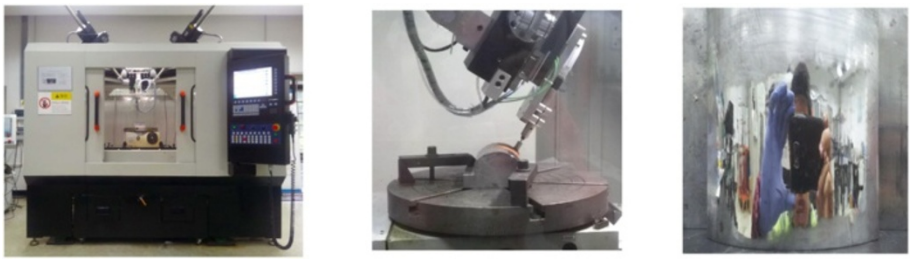

(a) Polishing machine (b) Polishing process (c) Polished surface

Figure 20 Automatic mechanical polishing of Bézier freeform surface. (a) Polishing machine. **(b)** Polishing process. **(c)** Polishing surface.

the Figure 14. Although this is the optimized result, the removed amount near the center of Archimedean spiral is still highly asymmetric.

Hilbert fractal polishing path

The quintic Hilbert fractal curve is projected on a plane with the range $[-2R, 2R] \times [-2R, 2R]$. In order to ignore the boundary effect, only the results in the area within the range $[-R, R] \times [-R, R]$ are studied. The polishing space of small segment line in the quintic Hilbert fractal curve is $0.125R$. Figure 17 is the polishing removal function curve of the quintic Hilbert fractal curve along the X-axis. It can be seen from the figure that the removal amount is symmetrical to the Y-axis. In addition, the periodic of the polishing removal function is not obvious, which means it satisfies the overall randomness requirement of polishing.

The overall randomness characteristic of the fractal curve polishing path can be seen from the three-dimensional graph of the removal function which is shown in Figure 18. This kind of characteristic is very suitable for surface polishing, and it can make the polishing results achieve good performance.

Experiment

The features for the three kinds of polishing path are listed in Table 1. Thus, the polishing path selected in this study is the Hilbert fractal polishing path which has geometric ergodicity and affine projection invariance characteristics.

In order to verify the performance of the presented polishing path, a part with Bézier freeform surface is selected. First, the discrete point positions and their normal vectors of the surface are saved. Next, by importing them into the fractal path generation module developed with Equation 31, the Hilbert fractal path is obtained. Then, the data file of the Hilbert fractal path is imported into the polishing simulation software of the self-developed polishing machine and the path on the freeform surface is obtained, which is shown in Figure 19.

Based on the freeform surface polishing requirement, a self-developed automatic polishing machine is proposed, which mainly includes a five-DOF parallel manipulator, a single DOF rotary table, and a linear motion platform with a force feedback system. It has been described extensively elsewhere in the literatures [26-28]. The parallel manipulator is a closed mechanical structure, and it has high stiffness, low inertia, and high dynamic performance. In the polishing process, the high stiffness helps to reduce the vibration generated by high speed rotation of polishing spindle, and the low inertia feature allows high polishing speed. A redundant translation is provided by

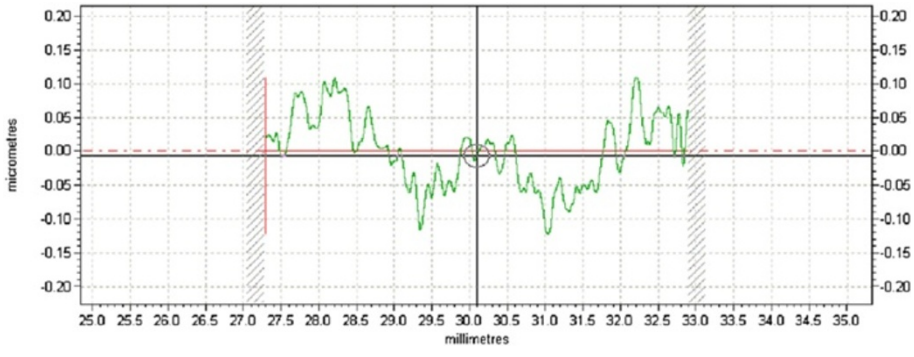

Figure 21 Roughness of polished surface.

a linear motion actuator on the moving platform to realize a constant polishing force. The rotary table is used to enlarge the polishing workspace of the automatic polishing machine. Moreover, with the help of rotary table, the path generation module could generate a singular-free and optimized dexterity polishing path for the parallel manipulator. Wool wheel polishing tool and polishing paste are used to polish the freeform surface part. During the experiment, the objective constant control force is set as 6N, and the polishing process is shown in Figure 20.

The roughness of the part surface is detected by the Taylor Hobson roughmeter. The original surface is only dealt with polishing cloth, and the roughness S_a equals 173.5 nm and the maximum height of the profile S_z equals 383.9 nm. This belongs to level 9 precision. After polishing, the roughness S_a decrease to 43.1 nm and the maximum height of the profile S_z decrease to 119.4 nm. This belongs to level 11 precision. The measuring roughness of the freeform surface after polishing is demonstrated in Figure 21.

Conclusions

Path planning is one of the key issues of the polishing process for freeform surface. Using the classical Preston polishing function, the mathematical model of small polishing tool is derived. With the assumption of a constant polishing pressure, the removal functions of scan line polishing path, Archimedean spiral polishing path, and Hilbert fractal polishing path are derived. The modeling method for polishing paths on a planar surface projected on a freeform surface is also discussed.

As different parameters for the same type polishing path may cause different polishing quality, the optimize parameters of polishing path are analyzed. The optimal polishing space for the scan line path and the Archimedean spiral polishing path is $1.9R$ and $1.3R$, respectively. By comparing the removal functions of different polishing path, the reasonable polishing path and parameters are chosen. In order to verify the effectiveness of the selected Hilbert fractal polishing path, a polishing experiment is conducted on a self-developed mechanical polishing machine and the sequence of polishing process can be automatically scheduled. The results demonstrate that the roughness of freeform surface is improved from level 9 to level 11.

Competing interests

The authors declare that they have no competing interests.

Authors' contributions

WL carried out all the simulations and developed the polishing machine. PX drafted the manuscript and participated in the polishing experiment. BL conceived the study and participated in its design and coordination. XY participated in the polishing experiment. All authors read and approved the final manuscript.

Acknowledgements

This work was supported in part by the National Science Foundation under grant 51175105 and in part by the Research Projects of Shenzhen under grant numbers JCYJ20140417172417129 and SGLH20131010144128266.

Author details

[1]Shenzhen Graduate School, Harbin Institute of Technology, Shenzhen University Town, Xili, 518055 Shenzhen, China. [2]School of Astronautics, Harbin Institute of Technology, Xidazhi Street, 150001 Harbin, China. [3]Mechanical Automation of Engineering, the Chinese University of Hong Kong, NT Road, 999077 Shatin, Hong Kong. [4]Department of Industrial and Systems Engineering, the Hong Kong Polytechnic University, Yuk Choi Road, 999077 Kowloon, Hong Kong.

Received: 25 October 2014 Accepted: 1 December 2014
Published online: 30 December 2014

References

1. Tsai MJ, Chang J-L, Haung J-F (2005) Development of an automatic mold polishing system. Automation Sci Eng IEEE Trans 2(4):393–397
2. Kao P, Hocheng H (2003) Optimization of electrochemical polishing of stainless steel by grey relational analysis. J Mater Process Technol 140(1):255–259
3. Kordonski WI, Jacobs S (1996) Magnetorheological finishing. Int J Modern Phys B 10(23n24):2837–2848
4. Sidpara A, Jain V (2011) Experimental investigations into forces during magnetorheological fluid based finishing process. Int J Mach Tools Manufacture 51(4):358–362
5. Wang B, Zhang J, Dong S (2009) New development of atmospheric pressure plasma polishing. Chinese Optics Lett 7(6):537–538
6. Yamamura K, Takiguchi T, Ueda M, Deng H, Hattori A, Zettsu N (2011) Plasma assisted polishing of single crystal SiC for obtaining atomically flat strain-free surface. CIRP Annals-Manufacturing Technol 60(1):571–574
7. Zhao J, Zhan J, Jin R, Tao M (2000) An oblique ultrasonic polishing method by robot for free-formsurfaces. Int J Mach Tools Manufacture 40(6):795–808
8. Zhao M, Li Y, Kao HT (2012) Design and dynamic analysis of horn for ultrasonic polishing. Appl Mech Mater 121:2619–2623
9. Cheung C, Kong L, Ho L, To S (2011) Modelling and simulation of structure surface generation using computer controlled ultra-precision polishing. Precision Eng 35(4):574–590
10. Shu Y, Nie X, Shi F, Li S (2014) Smoothing evolution model for computer controlled optical surfacing. J Optical Technol 81(3):164–167
11. Zhan J, Zhao J, Xu S, Zhu P (2002) Study of the contact force in free-form-surfaces compliant EDM polishing by robot. J Mater Process Technol 129(1):186–189
12. Jones RA (1977) Optimization of computer controlled polishing. Appl Optics 16(1):218–224
13. Tam H-y, Cheng H (2010) An investigation of the effects of the tool path on the removal of material in polishing. J Mater Process Technol 210(5):807–818
14. Wang W, Yun C (2011) A path planning method for robotic belt surface grinding. Chin J Aeronaut 24(4):520–526
15. Zheng D, Lu F, Zhang LZ, Shi YJ (2012) The effect of polishing tool path on polishing parameters. Appl Mech Mater 101:1043–1046
16. Pan R, Yang W, Guo YB, Yang F, Zhang DX (2012) Research on the optimized tool-path planning of computer controlled optical surfacing. Adv Mater Res 399:1763–1767
17. Rososhansky M, Xi FJ (2011) Coverage based tool-path planning for automated polishing using contact mechanics theory. J Manufacturing Syst 30(3):144–153
18. Marinescu ID, Uhlmann E, Doi T (2006) Handbook of lapping and polishing. CRC Press, New York
19. Tsai M-J, Fang J, Chang J-L (2006) Robotic path planning for an automatic mold polishing system. Int J Robot Automation 19(2):81–90
20. Li H, Walker D, Yu G, Zhang W (2013) Modeling and validation of polishing tool influence functions for manufacturing segments for an extremely large telescope. Appl Optics 52(23):5781–5787
21. Tam H-y, Cheng H (2010) An investigation of the effects of the tool path on the removal of material in polishing. J Mater Process Technol 210(5):807–818

22. Lambropoulos JC, Jacobs SD, Ruckman J (1999) Material removal mechanisms from grinding to polishing. Ceram Trans 102:113–128
23. Lin S-C, Wu M-L (2002) A study of the effects of polishing parameters on material removal rate and non-uniformity. Int J Mach Tools Manufacture 42(1):99–103
24. Tseng W-T, Wang Y-L (1997) Re-examination of pressure and speed dependences of removal rate during chemical-mechanical polishing processes. J Electrochemical Soc 144(2):15–17
25. Nanz G, Camilletti LE (1995) Modeling of chemical-mechanical polishing: a review. Semiconductor Manufacturing IEEE Trans 8(4):382–389
26. Li B, Lin W, Yang X, Deng Z (2010) Kinematic analysis and design for a 4URHU-1URHR parallel kinematic polishing machine. In: Proceedings of CLAWAR. World Scientific, Nagoya, Japan
27. Lin W, Li B, Yang X, Zhang D (2013) Modelling and control of inverse dynamics for a 5-DOF parallel kinematic polishing machine. Int J Advanced Robot Syst 10:1–21
28. Li B, Li G, Lin W, Xu P (2014) Design and constant force control of a parallel polishing machine. In: Information Science and Technology (ICIST), 2014 4th IEEE International Conference On, IEEE, Shenzhen, China, pp 324–328